

# Theory and Design of THz Intracavity Gain-Flattened Filters for Monolithically Integrated Mode-Locked Lasers

John S. Parker, Robert S. Guzzon, Erik J. Norberg, Ashish Bhardwaj,  
Pietro R. A. Binetti, and Larry A. Coldren, *Fellow, IEEE*

**Abstract**—We present the theory and design of a tunable gain-flattening filter for integrated mode-locked lasers (MLLs). The filter provides the inverse of the semiconductor spectral gain profile and produces a broad flattened net gain. This improves the performance of MLLs by allowing more modes to lase simultaneously. We demonstrate a gain-flattened MLL with a record 10 dB bandwidth of 2.08 THz, the widest frequency comb span for an integrated quantum-well-based laser at 1.55  $\mu\text{m}$ . Gain-flattening theory is used to extend the integrated comb span to 40 nm. We use scattering matrices to investigate feed-forward filters based on asymmetric Mach–Zehnder interferometers (MZIs). We compare MZI filters designed for a fixed coupling value to those that use an active gain arm to adjust the extinction ratio. Tunable zero placement of these filters is achieved using a passive phase tuning arm. The optimized gain-flattening filter has a 5 dB extinction ratio and a 70 nm free-spectral-range. When the filter is incorporated into a ring MLL, simulations predict a 40 nm, i.e., 5 THz, comb span with a power variation <3.5 dB.

**Index Terms**—Integrated optics, mode-locked lasers, optical filters, photonic integrated circuits, quantum well devices, quantum well lasers, semiconductor laser, semiconductor optical amplifier.

## I. INTRODUCTION

A FLATTENED gain spectrum is highly beneficial to photonic components in a wavelength division multiplexed (WDM) system, including: broadband amplifiers [1], tunable lasers [2], and multiwavelength sources such as mode-locked lasers (MLL) [3]. MLLs can provide low-noise and narrow linewidth phase-locked comb-lines with a set frequency spacing for applications including: optical signal processing [4], coherent communication [5], and spectroscopy [6]. Additionally, emerging applications in integrated laser offset locking

Manuscript received August 1, 2011; revised September 27, 2011; accepted October 22, 2011. Date of current version January 24, 2012. This work was supported in part by the Defense Advanced Research Projects Agency Photonic Integration for Coherent Optics Program. A portion of this work was done in the UCSB Nanofabrication Facility, part of the National Science Foundation funded National Nanotechnology Infrastructure Network.

J. S. Parker, R. S. Guzzon, E. J. Norberg, P. R. A. Binetti, and L. A. Coldren are with the Department of Electrical Engineering, University of California, Santa Barbara, CA 93106 USA (e-mail: JJSParker@gmail.com; rob.guzzon@gmail.com; norberg@ece.ucsb.edu; pbinetti@gmail.com; coldren@ece.ucsb.edu).

A. Bhardwaj was with the Department of Electrical and Computer Engineering, University of California, Santa Barbara, CA 93106 USA. He is now with JDS Uniphase Corporation, San Jose, CA 95134 USA (e-mail: Ashish.Bhardwaj@jdsu.com).

Color versions of one or more of the figures in this paper are available online at <http://ieeexplore.ieee.org>.

Digital Object Identifier 10.1109/JQE.2011.2174199

require a broadband stable frequency comb-line reference, which can be generated using a gain flattened mode-locked laser [7], [8]. However, the span of the frequency comb generated in integrated MLLs is limited by cavity dispersion and the flatness of the gain spectrum. The cavity dispersion is typically low for InP based material and can be compensated for by using an arrayed waveguide grating (AWG), or by optimizing the drive current and absorber bias of the MLL [9], [10]. Therefore, the generation of a flattened gain spectrum is crucial to improving the performance of MLLs. In this paper, we analyze the design of intracavity filters for enhanced gain flatness. To the best of our knowledge, this is the first paper on the design of intracavity integrated gain-flattening filters.

A flattened gain profile equalizes the output power at multiple wavelengths creating a more uniform comb across an optical band. Taking a broad historical view, two general approaches have been pursued: type I used material growth, whereas type II used filters to add loss at the peak gain.

Initial type I gain-flattening was focused on custom materials for WDM erbium-doped fiber amplifiers (EDFAs). In the early 1990's, experiments on EDFAs that used fluorozirconate glass instead of the standard silica core demonstrated improved gain flatness with <2 dB gain ripple over 30 nm bandwidth [11]. Such type I solutions had several advantages, including simplicity and power efficiency by avoiding a lossy external filter element.

For integrated devices, type I solutions have focused on tailoring the gain of the semiconductor material. For example, asymmetric quantum wells have been studied extensively on the InGaAs/GaAs and InGaAsP/InP material platforms, where a flat gain bandwidth with 1 dB ripple across 90 nm has been demonstrated [12]. These structures have used multiple quantum wells with different bandgaps to achieve flat gain profiles. While asymmetric quantum wells have shown promising results, the gain profile is highly dependent on pump current and the uniformity of the carrier distribution across the quantum wells [13]. Thus broad gain is only achievable over a narrow range of pump currents, or conversely, at a fixed gain. Additionally, devices based on asymmetric quantum wells are very sensitive to changes in material growth and operating temperature.

In type II gain-flattening approaches based on filters, bench-top EDFAs with thin film filters have been studied extensively, and commercial modules are readily available to flatten

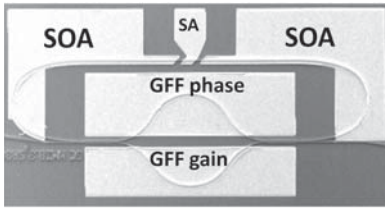


Fig. 1. Fabricated mode-locked laser with a gain-flattening filter (GFF).

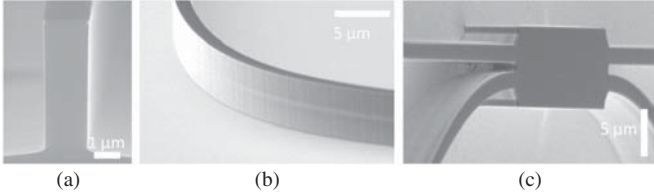


Fig. 2. Scanning electron microscope (SEM) images of the etched waveguide showing (a)  $5\ \mu\text{m}$  deep etch with vertical sidewalls, (b) waveguide bends with smooth sidewalls, and (c) multimode interference (MMI) couplers.

the EDFA output. Prior to this, Bragg filters and acousto-optic filters were also studied for bench-top gain-flattening [14], [15]. Researchers have demonstrated broadband comb generation using bench-top gain flattened mode-locked laser by incorporating a spectrometer and spatial filter into their free-space optical set-up [16]. For integrated devices, silicon planar lightwave circuits (PLCs) have been demonstrated for EDFA gain-flattening [17]. Yet there has been minimal research done on integrated gain-flattening filters for use in mode-locked lasers.

Recently, we demonstrated an integrated intracavity gain-flattening filter (GFF) on InGaAsP/InP that doubled the locking bandwidth of a ring MLL [18], and provided far wider comb spans than any simple non-gain-flattened ring MLL fabricated on the same material platform [19]. The filter was an asymmetric Mach-Zehnder interferometer (MZI).

In this paper, we begin by demonstrating a  $-10\ \text{dB}$  bandwidth of 2.08 THz from the MZI-MLL. We were able to operate this device at a higher current density than our previous devices due to better metal evaporation and a lower p-type contact resistance, thus breaking our prior 1.8 THz record, and producing the widest frequency comb that has yet been generated from an integrated quantum well (QW) based MLL at  $1.55\ \mu\text{m}$  [19], [20]. In the remainder of the paper, we discuss the design optimization of monolithically integrated intracavity GFFs, targeting 5 THz, i.e. 40 nm, flattened gain bandwidth. We develop a general analytical formulism for calculating the change in threshold current density and the output power due to an intracavity gain flattening filter. Based on this approach, in the ideal case we show that the bandwidth can be flattened up to 40 nm with  $\sim 10\%$  reduction in the total output power. We use scattering matrices, to include the coupled cavity effects from incorporating an intracavity filter, and we compare MZIs designed for a fixed coupling value to those that use an active gain arm to adjust the extinction ratio. We show that for the optimized GFF incorporated into a ring mode-locked laser, simulations can achieve a 40 nm, i.e. 5 THz, comb span with a power variation  $< 3.5\ \text{dB}$ .

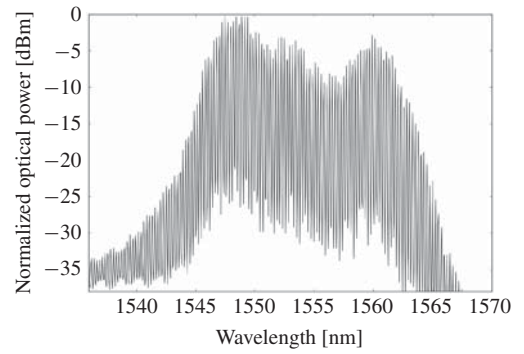


Fig. 3. Normalized optical power spectrum of optical comb generated from gain flattened mode-locked laser. The  $-10\ \text{dB}$  comb span is 16.75 nm (2.08 THz).

It is to be noted that such versatile filters can be tailored for any semiconductor gain material including: quantum wells (QWs), quantum dots (QD), or bulk. Hence, these filters can provide improved bandwidth for most integrated mode-locked lasers. Furthermore, these filters can be dynamically tuned to tailor the gain spectrum after fabrication to account for changes in material growth and operating temperature variations.

## II. FABRICATED GAIN-FLATTENED MODE-LOCKED LASER

The fabricated GFF-MLL is shown in Fig. 1. It has two 3 dB multimode interference (MMI) couplers with two arms that differ in length by  $16\ \mu\text{m}$  to form an intracavity asymmetric MZI; this filter has a free-spectral-range (FSR) of 39.7 nm. The MLL has a round-trip cavity length of  $2600\ \mu\text{m}$  with two  $750\ \mu\text{m}$  long SOAs, and a  $60\ \mu\text{m}$  long SA. The GFF phase arm controls the filter's zero placement, while the GFF gain arm controls the filter's extinction ratio (ER).

This device is fabricated on an InGaAsP/InP offset quantum well (OQW) platform that contains seven 0.9% compressively strained QWs and eight  $-0.2\%$  tensile strained barriers that are epitaxially grown above a 300 nm 1.3Q InGaAsP layer as part of the base epi. Passive areas are defined by a selective wet-etch and a single blanket regrowth is used to cover the device with a  $\text{p}^+$ -doped InP cladding, a  $\text{p}^{++}$ -doped InGaAs contact layer, and an InP capping layer to protect the InGaAs contact layer during device fabrication. The active material is used to define the semiconductor optical amplifiers (SOAs) and the saturable absorber (SA), whereas the passive material is used to define the low-loss waveguides and current injection based phase shifters.

After regrowth, the waveguide is defined with photoresist on a Cr/SiO<sub>2</sub> bilayer hard mask. The Cr is etched using a low power Cl<sub>2</sub>-based inductively coupled plasma (ICP), and the SiO<sub>2</sub> is etched using an SF<sub>6</sub>/Ar based ICP. The resulting 600 nm SiO<sub>2</sub> mask acts as a hard-mask to define the InGaAsP/InP deeply etched waveguides using a Cl<sub>2</sub>/H<sub>2</sub>/Ar (9/18/2 sccm) ICP at a chamber pressure of 1.5 mT. The resulting etched features are shown in Fig. 2. After removing the SiO<sub>2</sub> mask, blanket deposition of a 350 nm isolation layer of silicon nitride is performed. Vias are opened for

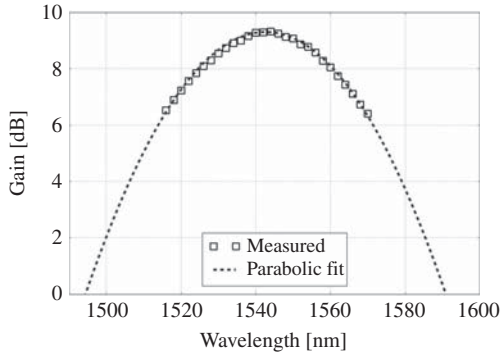


Fig. 4. Measured and parabolic fit gain spectrum. Parabolic fit [dB] =  $9.3 - (1543 - \lambda)^2 / 250$ .

topside p-metal contacts. N-metal contacts are realized through backside deposition of Ti/Pt/Au onto the n-doped conducting InP substrate. For more details on the fabrication and testing of the MLL-GFF, see [20].

When operating at 210 mA drive current,  $-2.1$  V saturable absorber bias, 35 mA GFF gain current, and 15.5 mA GFF phase current, this device provides a  $-10$  dB lasing bandwidth as wide as 16.75 nm, more than 2 THz, as shown in Fig. 3. Nevertheless, the flattened gain bandwidth can be improved further as this standard 7 QW material platform has more than 100 nm of positive gain bandwidth. In the next section, we examine intracavity gain-flattening using an ideal GFF, and then in Section IV and V using a realistic single-stage filter that can be monolithically integrated on InGaAsP/InP.

### III. IDEAL PARABOLIC GAIN-FLATTENING FILTER

Semiconductor gain material has a near-parabolic gain profile due to the curvature of the valence and conduction bands. The parabolic profile fits well near the peak gain and deviates as the gain approaches transparency. The measured and parabolic fit for standard 7 offset-quantum well (OQW) gain material is shown in Fig. 4.

The gain peak is at 1543 nm and fits well to a parabola over a 50 nm range from 1518–1568 nm. The gain is measured by fiber coupling a 1 mW tunable laser into the input waveguide. Three 400  $\mu\text{m}$  long SOAs are positioned serially along the waveguide. The first two are reverse biased at  $-3$  V, and therefore act as photodetectors to record the input power from the tunable laser; the second SOA absorbs any light that is not captured in the first section. Then, the first SOA is forward biased, and the second and third SOAs are reverse biased at  $-3$  V to record the amplified power. The peak gain is measured at  $\sim 4$  kA/cm<sup>2</sup> for the 400  $\mu\text{m}$   $\times$  1.8  $\mu\text{m}$  SOA.

In the following mathematical derivation, we will use this parabolic fit to calculate the change in threshold gain and output laser power as we introduce an ideal GFF. The parabolic gain approximation for a 400  $\mu\text{m}$  long SOA operating below saturation is calculated to be

$$g_{\text{SOA}, L=400 \mu\text{m}}(\lambda) = \left( 9.3 - \frac{(1543 - \lambda)^2}{250} \right) \text{dB} \quad (1)$$

where  $\lambda$  is the wavelength in nm.

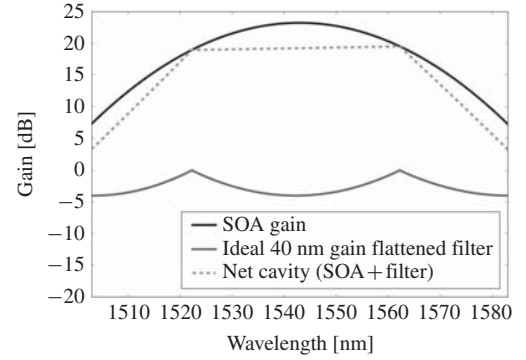


Fig. 5. Net cavity gain after insertion of ideal inverse parabolic gain-flattening filter.

Gain roll-off is the reduction in gain away from the peak gain wavelength, and it is represented by the denominator in the parabolic approximation. Furthermore, gain roll-off is proportional to the modal gain at the peak wavelength ( $g_{\text{peak}}$ ), as is clearly evident since the SOA's positive gain bandwidth (i.e. gain above transparency) does not change with SOA length. For example, the OQW SOA at a current density of 4 kA/cm<sup>2</sup> has positive gain over a 96 nm span regardless of SOA length. However, the peak gain ( $g_{\text{peak}}$ ) increases with length, hence, gain roll-off must increase with  $g_{\text{peak}}$ . A longer (or higher confinement factor) SOA will have a larger gain roll-off than a shorter (or lower confinement factor) SOA with the same current density. We define the SOA gain based on  $g_{\text{peak}}$  such that it is independent of length.

$$g_{\text{SOA}}(\lambda) = \left( g(N) - \frac{g_{\text{peak}}(\lambda_0 - \lambda)^2}{C_1} \right) \text{dB} \quad (2)$$

where  $g$  is a function of the carrier density,  $N$ , such that the maximum of  $g(N) = g_{\text{peak}}$ , and the parabolic gain roll-off coefficient is defined from Fig. 4 as  $C_1 = 250 \times 9.3$  [nm<sup>2</sup>]. For critical flat gain applications, such as mode-locked lasers, we want the largest ratio of gain/roll-off. Based on (2), this can be achieved by driving the SOA near its peak gain when lasing. As gain clamping restricts the increase of gain above lasing, we aim to use the shortest SOA that allows the cavity to lase. We can define a net cavity gain that includes SOA gain and the added wavelength dependence of the filter

$$\begin{aligned} g_{\text{Net}}(\lambda) &= g_{\text{SOA}}(\lambda) - \text{loss}_{\text{Filter}}(\lambda) \\ \therefore g_{\text{Net}}(\lambda) &= g_{\text{SOA}}(\lambda) + g_{\text{Filter}}(\lambda) \end{aligned} \quad (3)$$

where the wavelength dependent loss is defined as a negative filter gain. The net gain per cavity round-trip is a function of the SOA gain profile and the filter transfer function. For the parabolic SOA profile shown in Fig. 4, the ideal GFF will have an inverse parabolic shape, as shown in Fig. 5.

The applied filter is assumed to have a periodic transfer function. The free-spectral-range (FSR) of the filter determines the bandwidth of the flattened gain region. The filter adds loss at the peak of the gain profile to equalize the gain. Therefore, to create a wider flat bandwidth, the ER of the filter must be increased. For a laser cavity, this results in a higher threshold gain and lower output power.

We can now calculate the increase in threshold gain with an ideal GFF. For a cavity resonator, the  $g(N)$  term can be replaced with the threshold gain,  $g_{th}$ , as  $g(N)$  does not change above lasing threshold. For a ring MLL, the nominal threshold gain (i.e. without the GFF turned on) can be calculated from the measured losses of each element in the ring. The internal losses measured from cleave back tests [21] on Fabry-Perot lasers are 3.5 dB/mm passive material internal loss and 4.3 dB/mm active material internal loss. We assume a minimum of two 3 dB couplers are necessary to create the GFF, each with measured insertion loss  $<1$  dB. The saturable absorber (SA) loss is measured from a fabricated device to be  $\sim 1$  dB from injecting the output pulses from the MLL, in [18], into a saturable absorber test structure, and measuring CW power on the SA and an 800  $\mu\text{m}$  reversed biased SOA detector placed after it.

The nominal threshold gain ( $g_{th0}$ ) for a 2600  $\mu\text{m}$  circumference cavity with 1500  $\mu\text{m}$  length active and 1100  $\mu\text{m}$  length passive material is calculated as: internal loss + mirror loss (coupler transmission) + couplers insertion loss + SA loss = 10.3 dB + 3 dB + 2 dB + 1 dB = 16.3 dB. Assuming we have an ideal parabolic gain flattened filter, we can write the increased threshold gain ( $g_{th1}$ ) after gain-flattening as

$$g_{th0}(\Delta\lambda) = \left( g_{th1} - \frac{g_{peak}(\Delta\lambda/2)^2}{C_1} \right) \text{dB} \quad (4)$$

where  $\Delta\lambda$  is the gain flattened bandwidth.

We have replaced  $g(N)$  with the new threshold gain after gain-flattening,  $g_{th1}$ . The gain at the edge of the gain flattened spectrum must be increased to equal to the previous peak wavelength gain,  $g_{th0}$ , to maintain lasing, i.e. the gain at  $\lambda_0 + \Delta\lambda/2$  must be equal to the previous nominal threshold gain  $g_{th0}$ . However, we would like to define this expression in terms of  $g_{th1}$  to solve for the change in laser output power. Solving for  $g_{th1}$ , we calculate

$$g_{th1}(g_{th0}, \Delta\lambda) = g_{th0} + \frac{g_{peak}(\Delta\lambda/2)^2}{C_1}. \quad (5)$$

Using a logarithmic gain model [22], the threshold current density is related to the threshold gain by

$$J_{th1} = J_{tr} \exp(g_{th1}/g_0) \left[ \text{A/cm}^2 \right] \quad (6)$$

where the  $J_{th1}$  and  $J_{tr}$  terms are the threshold and transparency current density respectively. The  $g_{th1}$  and  $g_0$  terms are the threshold gain and gain constant respectively.  $A$  is the area of the active region in  $\text{cm}^2$  (length  $\times$  width). The output power [23] for a semiconductor laser is given by

$$P_{out1}(I_{th}) = \eta_d \eta_i \frac{h\nu}{q} (I - I_{th}) \quad (7)$$

$$P_{out1}(J_{th}) = \eta_d \frac{h\nu}{q} A (J - J_{th}) \quad (8)$$

where  $\eta_d$  is the differential efficiency and  $\eta_i$  is the injection efficiency. We find the change in cavity output power by combining (5), (6), and (8)

$$P_{out} = \eta_d \frac{h\nu}{q} A \left( J - J_{tr} \exp \left( \frac{g_{th0} + g_{peak}(\Delta\lambda/2)^2}{C_1 g_0} \right) \right). \quad (9)$$

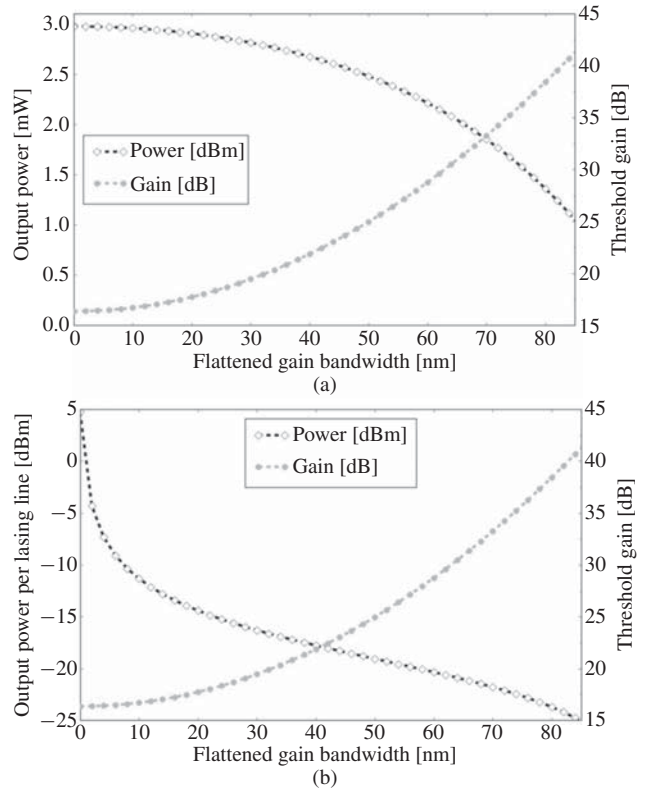


Fig. 6. (a) Laser output power and threshold gain versus flattened bandwidth of an ideal GFF. A larger flattened bandwidth requires added loss at the peak gain wavelength, increasing the threshold gain, and reducing the output power. The SOA drive current is fixed at 54 mA. The 40 nm flattened bandwidth has a 10% reduction in output power. (b) Output power per lasing line versus flattened bandwidth, assuming all modes within the flattened bandwidth lase. The output power per lasing line at 40 nm bandwidth is 22 dB lower than when the device operates with a single mode, i.e., 0 nm bandwidth.

The resulting plot of threshold gain and output power vs. gain flattened bandwidth is shown in Fig. 6(a). The drive current is held at 54 mA (e.g.  $3I_{th}$ ) whereas the nominal threshold current is 18 mA with a measured injection efficiency of 0.6 ( $J_{th} = 382 \text{ A/cm}^2$ ). For this material,  $J_{tr} = 31 \text{ A/cm}^2/\text{well}$  and  $g_0 = 650 \text{ cm}^{-1}$  are measured from broad-area laser cleave-back tests. Fig. 6(b) shows the output power in each of the lasing modes vs. gain flattened bandwidth. This plot uses the realistic assumption that all modes in the gain flattened bandwidth with equal round-trip gain are lasing simultaneously. The single lasing mode case occurs at 0 nm with 3 mW output, whereas at 40 nm flattened bandwidth there are 160 modes lasing with 20  $\mu\text{W}$  per lasing line output power. At 40 nm bandwidth, the output power is divided amongst many lines resulting in greatly decreased power per line, see Fig. 6(b), whereas the total power is reduced only slightly, see Fig. 6(a).

#### IV. MACH-ZEHNDER INTERFEROMETER GAIN-FLATTENING FILTER

In the previous section, we developed theory based on an ideal GFF. In this section, we examine a realistic single-stage GFF that can be monolithically integrated with minimal added components. For use in MLLs, we want to minimize the filter unit delay to avoid coherence effects in pulse propagation.

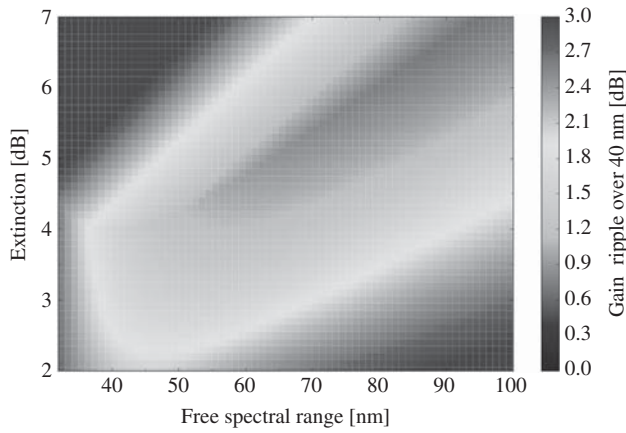


Fig. 7. Color map of gain ripple over a 40 nm bandwidth from variations in filter's extinction ratio and free spectral range.

For pulse widths of 1 ps we target delays  $\ll 1$  ps. This limits us to path length differences of  $\ll 80 \mu\text{m}$  in InP.

Feed-back filters, such as a coupled ring resonator, suffer from large loop delays much longer than the pulse width, which makes them unsuitable for short pulses. Feed-forward filters, such as a MZI, have short unit delays based on the difference in arm length. If we consider arms that differ in length by  $< 20 \mu\text{m}$  (i.e. one quarter of the pulse width), we calculate a filter FSR  $> 32 \text{ nm}$ . To compare MZI filter designs, the gain ripple (i.e. the maximum deviation in net gain) over a fixed 40 nm bandwidth is calculated for a range of FSR and ER, as shown in Fig. 7.

The filter flatness is improved as the FSR and ER are increased. Unlike the ideal GFF with an inverse parabolic profile, the MZI filter response matches the inverse parabola only near its center. Therefore, by increasing the FSR, the fit improves, however the threshold gain is increased as well due to a larger ER. The lowest ripple shown in Fig. 7 is 0.6 dB at an FSR of 100 nm with a 7 dB ER. However, by sacrificing a small amount of gain ripple we can use a lower ER, reduce the added loss from the applied filter, and operate with a lower threshold gain. By choosing 70 nm FSR, the optimal ER is 5 dB and the 40 nm gain ripple is 0.73 dB. The 70 nm FSR MZI filter response is shown in Fig. 8, along with the ideal inverse parabolic filter response. The ideal filter has an ER of 3.7 dB, whereas the optimized MZI filter is 1.3 dB greater.

This ER can be created by using equal power splitting couplers in the MZI with one variable amplitude arm by means of an SOA, or by using imbalanced power splitting couplers. The benefit of using the SOA is that variation to the ER can be made post-processing, which allows for dynamic control of the ER. However, a drawback of this approach is that the SOA in the amplitude arm is within the coupled-cavity system. Therefore, the carrier density in the amplitude arm cannot increase beyond the threshold carrier density of the laser before it gain-clamps, i.e. the gain per unit length cannot be higher in the amplitude filter arm than in the ring SOAs. This restricts the filter configurations. For example, consider a ring with a threshold gain of 15 dB with

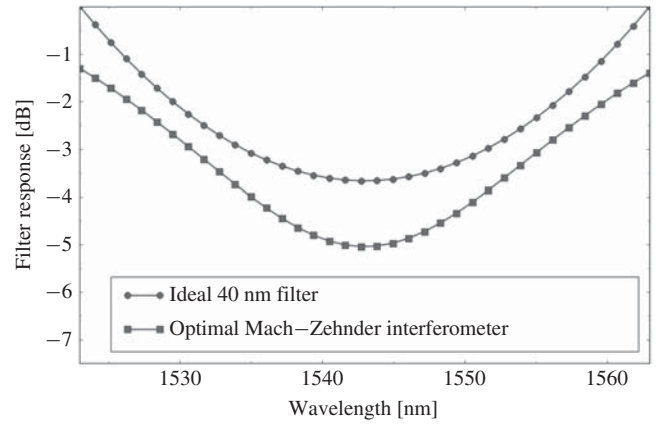


Fig. 8. Comparison of ideal gain-flattening filter and Mach-Zehnder interferometer filter response.

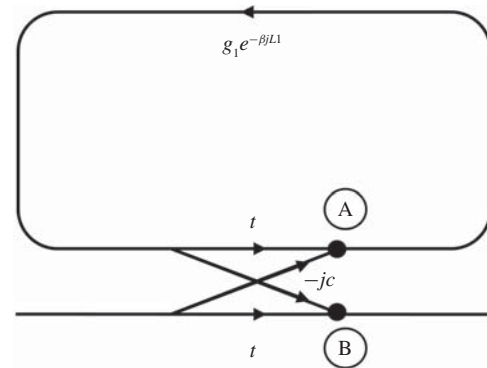


Fig. 9. Signal flow diagram of a single ring and coupler. Markers A and B designate nodes inside and outside of the ring cavity, respectively.

1500  $\mu\text{m}$  of SOA in the ring and filter arms with a length of 500  $\mu\text{m}$ . The maximum gain achievable in the amplitude filter arm would be approximately one-third of the threshold gain, i.e. 5 dB. When the gain arm is driven higher, its carrier density will clamp at  $N_{\text{th}}$ , preventing any further increase in gain.

For balanced power splitters, the desired 5 dB ER requires  $\sim 11$  dB power difference in both arms. Hence, to achieve a 40 nm flattened bandwidth the amplitude arm must only be used as an absorbing element rather than a gain element. This loss greatly increases the threshold gain, and for this reason the imbalanced coupler is preferred. Furthermore, the long SOA necessary to provide either 11 dB gain or loss in the filter arm has its own wavelength dependence based on the semiconductor gain medium.

The alternative to using a variable gain (loss) arm is to use imbalanced couplers. To achieve this 5 dB ER, fixed couplers with 78% power bar-coupling are required. Assuming a 1 dB processing tolerance on the ER (i.e.  $5 \pm 1$  dB, from Fig. 5), the fixed couplers must be between 75–82% bar-coupling. This can be achieved using reactive-ion etching (RIE) lag directional couplers, where two parallel deeply etched waveguides are separated by a narrow gap. This slows the etch rate between the waveguides and effectively forms a surface ridge directional coupler on a deeply etched waveguide in a single etch step. We have previously demonstrated RIE lag

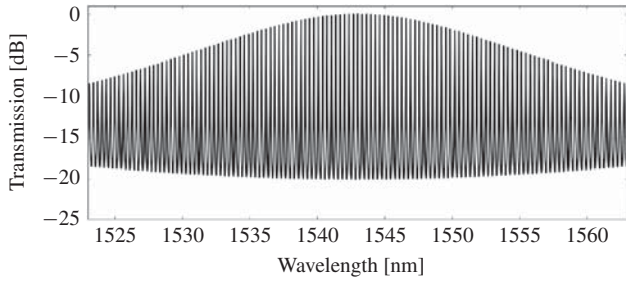


Fig. 10. Output power response of a single ring with coupler (A–B in Fig. 9). The variation in power response over the 40 nm spectrum is 8.5 dB.

directional couplers on non-gain-flattened ring mode-locked lasers with 90% bar-coupling, and we have shown that such couplers can be designed to provide arbitrary coupling from 1–99% [25]. Hence, the desired 5 THz comb generator using 78% couplers can be fabricated with realistic processing technology.

## V. GAIN FLATTENED FILTER COUPLED CAVITY MODEL

In the previous sections, we have analyzed the GFF as a component. The ideal GFF has been compared to a practical MZI filter that can be implemented in a monolithically integrated photonic circuit. However, when the GFF is placed inside a cavity, the filter response becomes more complex due to coupled-cavity effects, i.e. each MZI arm forms a resonant cavity with the larger ring. To simulate the effects of the filter in the cavity, we make use of scattering parameters to calculate the full coupled-cavity response. The signal flow diagram for a single ring and coupler is shown in Fig. 9; the coupler has bar-coupling ( $t$ ) and cross-coupling ( $-jc$ ).

The amplitude transfer function from A to B, i.e. the transfer function of amplified spontaneous emission generated inside the ring seen at the output of the ring, is calculated as

$$H_{A-B}(\lambda) = \frac{-jcg_1(\lambda)\exp(-j\beta L_1)}{1 - tg_1(\lambda)\exp(-j\beta L_1)}. \quad (10)$$

Shown in Fig. 10, the power transmission out of the ring is calculated from the magnitude squared of the amplitude transfer function. All transfer functions are calculated at a pole response of 20 dB, which is typical for a lasing resonator, i.e. peak to trough extinction ratio is 20 dB. In this single ring without a filter, the wavelength dependent gain of the SOA causes the output transmission to vary by 8.5 dB over the 40 nm bandwidth and the pole response is decreased from 20 dB to  $\sim 10$  dB.

A signal flow graph for the ring MLL with a GFF is shown in Fig. 11. This ring has two couplers. The ring path and two MZI arms have amplitude gains  $g_1$ ,  $g_2$ , and  $g_3$ .

The amplitude transfer function inside the ring (from A to A) is solved using Mason's rule [24]

$$H_{A-A}(\lambda) = \frac{-c^2M_1(\lambda)M_3(\lambda) + t^2M_1(\lambda)M_2(\lambda)}{1 - t^2M_1(\lambda)M_2(\lambda) + c^2M_1(\lambda)M_3(\lambda)} \quad (11)$$

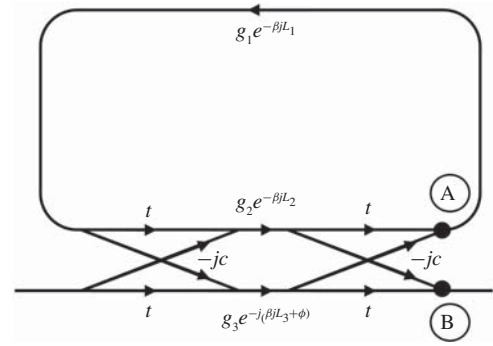


Fig. 11. Signal flow diagram of a ring with a gain-flattening filter. Markers A and B designate nodes inside and outside of the ring cavity, respectively.

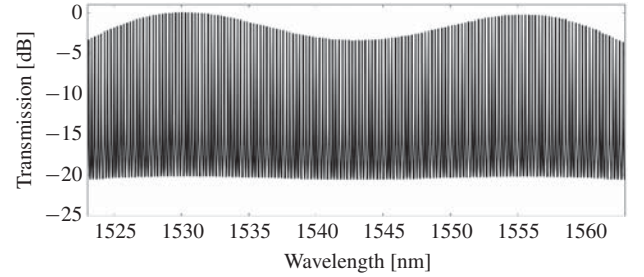


Fig. 12. Intracavity power response of a ring with a gain-flattening filter (A–A in Fig. 11). The variation in power response over the 40 nm spectrum is 3.4 dB.

$$M_1(\lambda) = g_1(\lambda)\exp(-j\beta L_1)$$

$$M_2(\lambda) = g_2(\lambda)\exp(-j\beta L_2)$$

$$M_3(\lambda) = g_3(\lambda)\exp(-j(\beta L_3 + \phi)).$$

The power transmission inside the ring with the GFF is plotted in Fig. 12. The small gain ripple calculated in Section IV by adding the filter and cavity gains is now enhanced by the resonant cavity operating at a high pole value of 0.82, i.e. a pole response magnitude of 20 dB. Over the 40 nm bandwidth, the 0.73 dB ripple in the net gain (calculated from the cascaded filter and SOA in Section IV) results in a 3.4 dB variation in the power response when these elements are placed inside a resonant cavity.

The response shown in Fig. 12 does not include the effect of coupling out of the cavity. To consider the output from the GFF-MLL, the transfer function from A to B is calculated as

$$H_{A-B}(\lambda) = \frac{-jctM_1(\lambda)M_3(\lambda) - jctM_1(\lambda)M_2(\lambda)}{1 - t^2M_1(\lambda)M_2(\lambda) + c^2M_1(\lambda)M_3(\lambda)}. \quad (12)$$

As shown in Fig. 12, the transfer function inside the ring (A–A) produces a flattened response compared to the single ring case, see Fig. 10. However, the output transfer function (A–B), as shown in Fig. 13, goes through the inverse GFF function when coupled out of the cavity. The transfer function (A–B) is degraded and the 40 nm transmission envelope has a 9.3 dB ripple, larger than the single ring by itself. Thus, while Fig. 13 achieves a flat response at the center of its comb, the comb profile falls off rapidly as it approaches the 40 nm bandwidth. To have the desired flat transfer function, covering the full 40 nm outside the cavity where it will be used, an

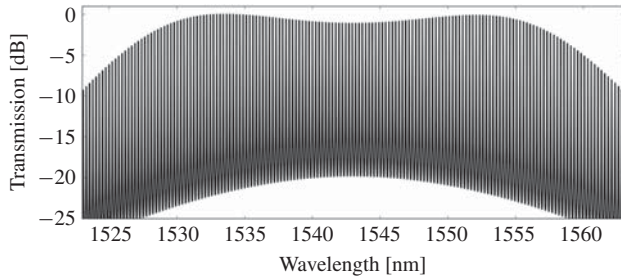


Fig. 13. Output power response of a ring with a gain-flattening filter (A–B in Fig. 11). The variation in power response over the 40 nm spectrum is 9.3 dB.

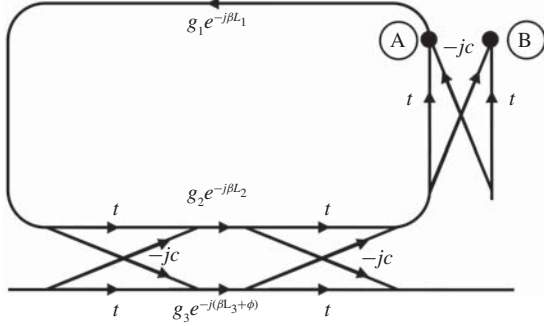


Fig. 14. Signal flow diagram of a ring with a gain-flattening filter and additional coupler. Markers A and B designate nodes inside and outside of the ring cavity respectively.

additional coupler is required to avoid passing the output comb spectrum through the inverse GFF. The cavity with an additional coupler is shown in Fig. 14 and shows the same spectral shape as Fig. 12, while in this case, the response is seen outside the ring. The draw-back of having an additional coupler is a slight increase in the threshold gain,  $\sim 2$  dB, for the 22% cross-coupling with 1 dB insertion loss used in this example.

The transfer function with the additional coupler is shown in Fig. 15 and calculated as

$$H_{A-B}(\lambda) = \frac{jc^3 M_1(\lambda) M_3(\lambda) - jct^2 M_1(\lambda) M_2(\lambda)}{1 - t^3 M_1(\lambda) M_2(\lambda) + tc^2 M_1(\lambda) M_3(\lambda)}. \quad (13)$$

All transfer functions have been calculated based on the fixed 5 dB filter ER calculated in Section IV. Compared to the single ring and coupler, the addition of the GFF results in a 7 dB increase in the threshold gain and a reduction in output power from 3.0 mW to 2.7 mW, as calculated in Fig. 6(a) (e.g. the increase in threshold gain = 5 dB from GFF + 2 dB from added coupler). Ring MLLs built on a QW gain platform have typical comb spans  $< 1$  THz [19], thus, the addition of the GFF reduces the laser output power by  $\sim 17\%$  while increasing the comb bandwidth by  $> 5$  X. However, the power per lasing line does decrease by  $> 85\%$  as the total output power is divided over more modes.

## VI. COMPARISON OF COUPLED CAVITY MODEL TO RESULTS

Using the coupled cavity model from Section V, we now compare the 2 THz measured comb from Fig. 3 to its simulated comb. The optical signal-to-noise ratio (OSNR) for the comb

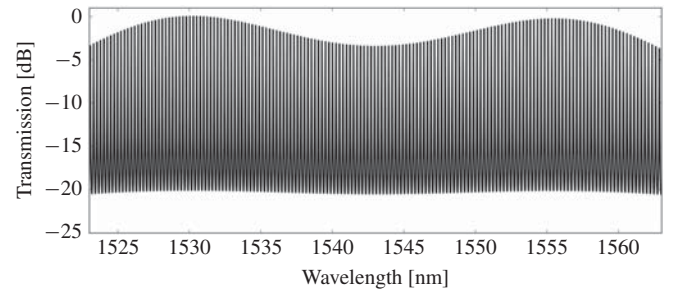


Fig. 15. Output power response of a ring with a gain-flattening filter and addition coupler (A–B in Fig. 14). The variation in power response over the 40 nm spectrum is 3.5 dB.

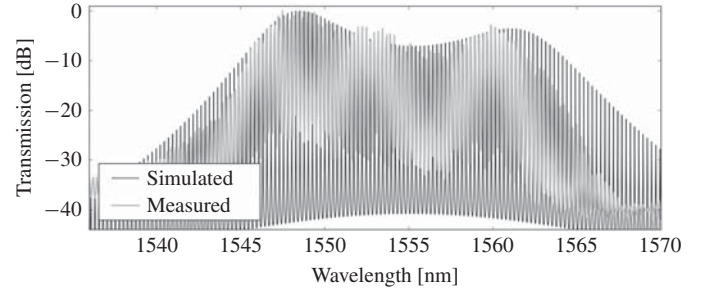


Fig. 16. Comparison of the measured and simulated power response from the gain-flattened mode-locked laser shown in Fig. 1. The  $-10$  dB bandwidth is 16.75 nm and 19 nm for the measured and simulated spectrums, respectively.

is 35–45 dB, measured over narrow 1 nm spans with a high resolution OSA. The pole magnitude of the coupled cavity response matches this OSNR. As shown in Fig. 16, the simulated and measured combs have similar spectral profiles, yet the span of simulated comb is 19 nm, which is 13% wider than the measured bandwidth. Such deviation is like due to the limitations of the model, as it does not include material dispersion or the time-dependent effects of the saturable absorber. Nevertheless, the simulated and measured comb profiles match well, indicating that the coupled cavity approach can provide a reasonable estimate for the flattened gain profile of a mode-locked laser.

## VII. CONCLUSION

We have demonstrated integrated gain-flattened MLLs with  $-10$  dB bandwidths of over 2 THz, which are the widest reported comb spans for QW based MLLs. We have developed an analytical formulism for the reduction in output power from a gain-flattened mode-locked laser. We have presented the theory and design of an integrated intracavity gain-flattening filter for a ring mode-locked laser that provides a 40 nm flattened comb span with less than 3.5 dB power variation. The ideal gain-flattening filter for quantum well semiconductor material is shown to have an inverse parabolic profile, which can be approximated well over a 40 nm span by a single Mach–Zehnder interferometer. An integrated gain flattened mode-locked laser can provide broad comb-line generation for use in laser offset locking, in spectroscopy, and as a compact coherent WDM source.

## REFERENCES

- [1] B. Clesca, D. Ronarc'h, D. Bayart, Y. Sorel, L. Hamon, M. Guibert, J. L. Beylat, J. F. Kerdiles, and M. Semenkoff, "Gain flatness comparison between erbium-doped fluoride and silica fiber amplifiers with wavelength-multiplexed signals," *IEEE Photon. Technol. Lett.*, vol. 6, no. 4, pp. 509–512, Apr. 1994.
- [2] L. A. Coldren, G. A. Fish, Y. Akulova, J. S. Barton, L. Johansson, and C. W. Coldren, "Tunable semiconductor lasers: A tutorial," *J. Lightw. Technol.*, vol. 22, no. 1, pp. 193–202, Jan. 2004.
- [3] H. Yasaka, Y. Yoshikuni, K. Sato, H. Ishii, and H. Sanjoh, "Multiwavelength light source with precise frequency spacing using mode-locked semiconductor laser and arrayed waveguide grating filter," in *Proc. IEEE Opt. Fiber Commun.*, Feb.–Mar. 1996, pp. 299–300.
- [4] P. J. Delfyett, S. Gee, M. T. Choi, H. Izadpanah, W. Lee, S. Ozharar, F. Quinlan, and T. Yilmaz, "Optical frequency combs from semiconductor lasers and applications in ultrawideband signal processing and communications," *J. Lightw. Technol.*, vol. 24, no. 7, pp. 2701–2719, Jul. 2006.
- [5] Y. B. M'Sallem, Q. T. Le, L. Bramerie, Q. Nguyen, E. Borgne, P. Besnard, A. Shen, F. Lelarge, S. LaRochelle, L. A. Rusch, and J. Simon, "Quantum-dash mode-locked laser as a source for 56-Gb/s DQPSK modulation in WDM multicast applications," *IEEE Photon. Technol. Lett.*, vol. 23, no. 7, pp. 453–455, Apr. 2011.
- [6] V. Gerginov, C. E. Tanner, S. A. Diddams, A. Bartels, and L. Hollberg, "High-resolution spectroscopy with a femtosecond laser frequency comb," *Opt. Lett.*, vol. 30, no. 13, pp. 1734–1736, 2005.
- [7] S. Ristic, A. Bhardwaj, M. J. Rodwell, L. A. Coldren, and L. A. Johansson, "An optical phase-locked loop photonic integrated circuit," *J. Lightw. Technol.*, vol. 28, no. 4, pp. 526–538, Feb. 2010.
- [8] C. F. C. Silva, A. J. Seeds, and P. J. Williams, "Terahertz span >60-channel exact frequency dense WDM source using comb generation and SG-DBR injection-locked laser filtering," *IEEE Photon. Technol. Lett.*, vol. 13, no. 4, pp. 370–372, Apr. 2001.
- [9] M. Kwakernaak, R. Schrieck, A. Neiger, H. Jackel, E. Gini, and W. Vogt, "Spectral phase measurement of mode-locked diode laser pulses by beating sidebands generated by electrooptical mixing," *IEEE Photon. Technol. Lett.*, vol. 12, no. 12, pp. 1677–1679, Dec. 2000.
- [10] M. J. R. Heck, P. Munoz, B. W. Tilma, E. A. J. M. Bente, Y. Barbarin, Y. S. Oei, R. Notzel, and M. K. Smit, "Design, fabrication and characterization of an InP-based tunable integrated optical pulse shaper," *IEEE J. Quantum Electron.*, vol. 44, no. 4, pp. 370–377, Apr. 2008.
- [11] D. Bayart, B. Clesca, L. Hamon, and J. L. Beylat, "Experimental investigation of the gain flatness characteristics for 1.55  $\mu\text{m}$  erbium-doped fluoride fiber amplifiers," *IEEE Photon. Technol. Lett.*, vol. 6, no. 5, pp. 613–615, May 1994.
- [12] O.-K. Kwon, K.-H. Kim, E.-D. Sim, J.-H. Kim, H.-S. Kim, and K.-R. Oh, "Asymmetric multiple-quantum-well laser diodes with wide and flat gain," *Opt. Lett.*, vol. 28, no. 22, pp. 2189–2191, 2003.
- [13] C.-F. Lin, B.-R. Wu, L.-W. Lai, and T.-T. Shih, "Sequence influence of nonidentical InGaAsP quantum wells on broadband characteristics of semiconductor optical amplifiers–superluminescent diodes," *Opt. Lett.*, vol. 26, no. 14, pp. 1099–1101, 2001.
- [14] P. F. Wysocki, J. B. Judkins, R. P. Espindola, M. Andrejco, and A. M. Vengsarkar, "Broad-band erbium-doped fiber amplifier flattened beyond 40 nm using long-period grating filter," *IEEE Photon. Technol. Lett.*, vol. 9, no. 10, pp. 1343–1345, Oct. 1997.
- [15] S. F. Su, R. Olshansky, D. A. Smith, and J. E. Baran, "Flattening of erbium-doped fibre amplifier gain spectrum using an acousto-optic tunable filter," *Electron. Lett.*, vol. 29, no. 5, pp. 477–478, Mar. 1993.
- [16] M. M. Mielke, G. A. Alphonse, and P. J. Delfyett, "Multiwavelength modelocked semiconductor lasers for photonic access network applications," *IEEE J. Sel. Areas Commun.*, vol. 25, no. 3, pp. 120–128, Apr. 2007.
- [17] K. Suzuki, T. Kitoh, S. Suzuki, Y. Inoue, Y. Hibino, T. Shibata, A. Mori, and M. Shimizu, "PLC-based dynamic gain equaliser consisting of integrated Mach-Zehnder interferometers with C- and L-band equalising range," *Electron. Lett.*, vol. 38, no. 18, pp. 1030–1031, Aug. 2002.
- [18] J. S. Parker, A. Bhardwaj, P. R. A. Binetti, Y.-J. Hung, C. Lin, and L. A. Coldren, "Integrated 30 GHz passive ring mode-locked laser with gain flattening filter," in *Proc. 22nd IEEE Int. Semicond. Laser Conf.*, Kyoto, Japan, Sep. 2010, no. PD1, pp. 1–2.
- [19] J. S. Parker, P. R. A. Binetti, A. Bhardwaj, R. S. Guzzon, E. J. Norberg, Y.-J. Hung, and L. A. Coldren, "Comparison of comb-line generation from InGaAsP/InP integrated ring mode-locked lasers," in *Proc. IEEE Conf. Lasers Electro-Opt.*, Baltimore, MD, May 2011, no. CTuV6, pp. 1–2.
- [20] J. S. Parker, A. Bhardwaj, P. R. A. Binetti, Y.-J. Hung, and L. A. Coldren, "Monolithically integrated gain-flattened ring mode-locked laser for comb-line generation," *IEEE Photon. Technol. Lett.*, to be published.
- [21] L. Coldren and S. Corzine, "A phenomenological approach to diode lasers," in *Diode Lasers and Photonic Integrated Circuits*, K. Chang, Ed. New York: Wiley, 1995, pp. 52–54.
- [22] L. Coldren and S. Corzine, "Gain and current relations," in *Diode Lasers and Photonic Integrated Circuits*, K. Chang, Ed. New York: Wiley, 1995, pp. 171–174.
- [23] L. Coldren and S. Corzine, "Dynamic effects," in *Diode Lasers and Photonic Integrated Circuits*, K. Chang, Ed. New York: Wiley, 1995, pp. 190–191.
- [24] J. S. Parker, P. R. A. Binetti, Y.-J. Hung, E. J. Norberg, and L. A. Coldren, "RIE lag directional coupler based integrated InGaAsP/InP ring mode-locked laser," in *Proc. 69th IEEE Annu. Device Res. Conf.*, Santa Barbara, CA, Jun. 2011, pp. 263–264.
- [25] S. J. Mason, "Feedback theory—further properties of signal flow graphs," *Proc. Inst. Rad. Eng.*, vol. 44, no. 7, pp. 920–926, Jul. 1956.



**John S. Parker** received the B.S. degree in engineering from Harvey Mudd College, Claremont, CA, in 2007, and the M.S. degree in electrical and computer engineering from the University of California, Santa Barbara, in 2009, where he is currently pursuing the Ph.D. degree.

His current research interests include radio-frequency photonics, coherent communication, and compact components for dense photonic integrated circuits.



**Robert S. Guzzon** received the B.S. degree in electrical engineering and physics from Lehigh University, Bethlehem, PA, in 2007. He is currently pursuing the Ph.D. degree in electrical engineering with the University of California, Santa Barbara.

His current research interests include the design and fabrication of versatile photonic integrated microwave filter systems that achieve high spurious free dynamic range, large-scale photonics integration, and microwave photonic signal processing.



**Erik J. Norberg** received the B.S. and M.S. degrees in engineering nanoscience from Lund University, Lund, Sweden, in 2008. He is currently pursuing the Ph.D. degree in electrical engineering with the University of California, Santa Barbara.

He is currently working on the development of high dynamic range integrated optical filters for microwave signal processing. His current research interests include the design and metalorganic chemical vapor deposition growth of large scale photonic integrated circuits on InP.



**Ashish Bhardwaj** received the B.Sc. (honors) and M.Sc. degrees in physics from the Indian Institute of Technology, Kharagpur, India, in 1994 and 1996, respectively, and the Ph.D. degree in applied physics from the California Institute of Technology, Pasadena, in 2001.

He was with the Bell Laboratories, Lucent Technologies, Holmdel, NJ, as a Technical Staff Member from 2001 to 2007, where he was engaged in research on fast wavelength switching in tunable lasers for applications in optical packet switching.

He also led research in the design, fabrication, and characterization of large-scale monolithically integrated InP-based photonic integrated circuits employing semiconductor optical amplifiers. From 2007 to 2011, he was with the Department of Electrical and Computer Engineering, University of California, Santa Barbara, where he led research in the design and fabrication of monolithically integrated optical phase-locked loops as coherent receivers for high dynamic range radio-frequency/photonic links. He is currently with JDS Uniphase Corporation, Milpitas, CA.



**Pietro R. A. Binetti** received the Ph.D. degree in electrical engineering from the COBRA Research Institute, Eindhoven University of Technology, Eindhoven, The Netherlands, in 2009.

He is currently a Post-Doctoral Fellow with the University of California, Santa Barbara. His current research interests include the design, fabrication, and characterization of photonic integrated circuits for analog and digital applications.



**Larry A. Coldren** (S'67–M'72–SM'77–F'82) received the Ph.D. degree in electrical engineering from Stanford University, Stanford, CA, in 1972.

He is the Fred Kavli Professor of optoelectronics and sensors with the University of California (UCSB), Santa Barbara. After 13 years in the research area with Bell Laboratories, Holmdel, NJ, he joined UCSB in 1984, where he is currently with the Department of Materials and the Department of Electrical and Computer Engineering. In 1990, he co-founded optical concepts, later acquired as Gore Photonics, to develop novel vertical-cavity surface-emitting laser (VCSEL) technology, and in 1998, he co-founded Agility Communications, Inc., Goleta, CA, later acquired by JDS Uniphase Corporation (JDSU), Milpitas, CA, to develop widely tunable integrated transmitters. At Bell Laboratories, he was initially on waveguided surface-acoustic-wave signal processing devices and coupled-resonator filters. He later developed tunable coupled-cavity lasers using novel reactive-ion etching technology that he created for the new InP-based materials. At UCSB, he continued work on multiple-section tunable lasers, in 1988, inventing the widely tunable multi-element mirror concept, which is currently used in some JDSU products. Near this time period, he also made seminal contributions to efficient VCSEL designs that continued to be implemented in practical devices till this day. More recently, his group has developed high-performance InP-based photonic integrated circuits as well as high-speed VCSELs, and they continue to advance the underlying materials growth and fabrication technologies. He has authored or co-authored over 1000 journals and conference papers, seven book chapters, and one textbook and has been issued 64 patents. He has presented dozens of invited and plenary talks at major conferences.

Prof. Coldren is a fellow of the Optical Society of America and a member of the National Academy of Engineering. He was a recipient of the John Tyndall and Aron Kressel Awards, in 2004 and 2009, respectively.